A classical theory for second-harmonic generation from metallic nanoparticles

Yong Zeng[1*], Walter Hoyer[2†], Jinjie Liu[1], Stephan W. Koch[2], Jerome V. Moloney[1]
1. Arizona Center for mathematical Sciences, University of Arizona, Tucson, Arizona 85721
2. Department of Physics and Material Sciences Center,
Philipps University, Renthof 5, D-35032 Marburg, Germany

In this article, we develop a *classical* electrodynamic theory to study the optical nonlinearities of metallic nanoparticles. The quasi-free electrons inside the metal are approximated as a classical Coulomb-interacting electron gas, and their motion under the excitation of an external electromagnetic field is described by the plasma equations. This theory is further tailored to study second-harmonic generation. Through detailed experiment-theory comparisons, we validate this classical theory as well as the associated numerical algorithm. It is demonstrated that our theory not only provides qualitative agreement with experiments, it also reproduces the overall strength of the experimentally observed second-harmonic signals.

PACS numbers: 42.70.-a, 52.35.Mw

I. INTRODUCTION

Optical second-harmonic generation (SHG) from a metal (silver) surface was first observed in 1965 [1], four years after the first observation of SHG from quartz in 1961 [2]. In the following fifty years, a number of important features of SHG from metallic surfaces have been founded such as (1) second harmonic (SH) intensities can be enhanced more than an order of magnitude by coupling incident light into surface polariton resonances at metal surfaces [3]; (2) SHG from surfaces of centrosymmetric metals is anisotropic, the strength of the SH response thus depends on the relative orientation of the incident field and the crystal axes [4, 5]; (3) Because of local-field enhancement, SHG is very sensitive to surface roughness and chemical processes such as adsorption and electrochemical reactions [6, 7]. On the theoretical side, different approaches on both phenomenological and microscopic levels have been developed to analyze SH response from metals [8], such as classical Boltzman equation approach [9], hydrodynamic model [10, 11, 12, 13, 14, 15], phenomenological formalism in terms of the fundamental tensor elements of the SH susceptibility [5, 6, 16, 17, 18, 19, 20, 21, 22] and the self-consistent density functional formalism (see Ref.[23, 24] and the cited references).

Recently, a renaissance of scientific interests appears in the quadratic nonlinearities of metallic nanostructures and nanoparticles (NPs) partially owing to the significant localizations of electromagnetic (EM) field induced by the plasmonic oscillations of the conduction electrons inside the metal [25, 26, 27, 28, 29, 30, 31, 32, 33, 34, 35, 36, 37, 38, 39, 40, 41, 42, 43, 44, 45, 46, 47]. More specifically, SHG were experimentally observed from different geometric configurations such as sharp metal tips [28, 32], periodic nanostructured metal films [29], imperfect spheres [31, 35], split-ring resonators [34, 40] and their complementary counterparts [42], metallodielectric multilayer photonic-band-gap structures [41], T-shaped [40] and L-shaped NPs [38, 43], noncentrosymmetric T-shaped nanodimers [39, 46] and "fishnet" structures [44].

It should be emphasized that these subwavelength NPs and one-dimensional interfaces have different structural symmetries, and these differences further lead to significant consequences. For ideally infinite interfaces, the dominant SH dipole source appears only at the interface between centrosymmetric media where the inversion symmetry is broken, although higher order multipole sources provide a relatively small bulk SH polarization density. The SH polarization density is thus significantly localized in a *surface* region a few Angstrom wide, and sensitively influenced by the details of the surface electronic structure. On the other hand, for low-symmetric or even asymmetric NPs, such as gold split-ring resonators, SH dipolar polarizability may be presented in the whole *volume* and not limited at the interface [48]. Consequently, the overall shape of the NP plays a significant role in determining the SH response. To analyze the quadratic nonlinearities of these metallic NPs, we therefore propose that complicated microscopic models of the interfaces are not required, and an easy-to-implement classical model is sufficient.

The paper is organized as follows. Section 2 presents a classical electrodynamic model which describes the nonlinearities induced by Coulomb-interacting electron gas in metals. Using small nonlinearity approximation, this classical model is further tailored in Section 3 to treat second-order generation. Section 4 gives a detailed comparison between

* zengy@acms.arizona.edu
† The first and second author contributes equally to this article.

theoretical results and the corresponding experiments. Discussion, conclusion and acknowledgement are presented in Section 5 and Section 6, respectively.

II. CLASSICAL ELECTRODYNAMIC MODEL

In our model, the motion of quasi-free electrons inside a metal is described classically. Quantum mechanical Coulomb correlations and exchange contributions are thus missing while the classical Coulomb interaction (i.e. the Hartree term in a quantum mechanical derivation) is fully included [49]. Furthermore, the Coulomb scattering due to higher-order quantum corrections is phenomenologically described via an inverse decay time $\gamma = 1/\tau$. The electrons inside the metal are described via their number density n_e and velocity $\mathbf{u}_e$. In our classical model, these quantities are continuous functions of position $\mathbf{r}$ and time t [50, 51, 52, 53]. We further assume the mass of ions are infinite. Consequently, the ionic density $n_0(\mathbf{r})$ is time-independent and only the electrons can move and contribute to the current density. In other words, an infinite barrier surface potential is assumed and $n_0(\mathbf{r})$ is constant within the metal and zero outside the metal.

We begin with two equations for electronic number density $n_e(\mathbf{r}, t)$ and the velocity field $\mathbf{u}_e(\mathbf{r})$,

$$\frac{\partial n_e}{\partial t} + \nabla \cdot (n_e \mathbf{u}_e) = 0, \tag{1}$$

$$m_e \left(\frac{\partial}{\partial t} + \mathbf{u}_e \cdot \nabla \right) \mathbf{u}_e = -e \left(\mathbf{E} + \mathbf{u}_e \times \mathbf{B} \right). \tag{2}$$

Here, the first equation is the usual continuity equation expressed in terms of carrier density instead of charge density. The second equation is the generalization of Newton's equation to the case of a continuous field. The term in brackets on the left-hand side is the so-called *convective* or *material* derivative, which is a result of the description of electrons in terms of a continuous density and can be formally derived from the quantum mechanical Wigner distribution [49]. More intuitively, it can be understood as the time derivative of an electron taken with respect to a coordinate system which is itself moving with velocity $\mathbf{u}_e(\mathbf{r}(t), t)$, given by [51]

$$\frac{d\mathbf{u}_e}{dt} = \frac{\partial \mathbf{u}_e}{\partial t} + \left[\frac{d\mathbf{r}(t)}{dt} \cdot \nabla \right] \mathbf{u}_e = \left(\frac{\partial}{\partial t} + \mathbf{u}_e \cdot \nabla \right) \mathbf{u}_e. \tag{3}$$

To describe the interaction between the classical electron gas and the external EM fields self-consistently, we couple Eqs. (1) and Eqs. (2) to Maxwell's equations by defining the charge density and the current density

$$\rho(\mathbf{r}, t) = e \left[n_0(\mathbf{r}) - n_e(\mathbf{r}, t) \right], \tag{4}$$

$$\mathbf{j}(\mathbf{r}, t) = -e n_e(\mathbf{r}, t) \mathbf{u}_e(\mathbf{r}, t) = \left[\rho(\mathbf{r}, t) - e n_0(\mathbf{r}) \right] \mathbf{u}_e(\mathbf{r}, t), \tag{5}$$

in terms of the electronic number density and velocity field. Using these definitions and the equations of motion, Eqs. (1) and Eqs. (2), we achieve

$$\frac{\partial \rho}{\partial t} = -\nabla \cdot \mathbf{j}, \tag{6}$$

$$\frac{\partial \mathbf{j}}{\partial t} = \sum_k \frac{\partial}{\partial r_k} \left(\frac{\mathbf{j} j_k}{e n_0 - \rho} \right) + \frac{e^2 n_0}{m_e} \mathbf{E} - \frac{e}{m_e} \left[\rho \mathbf{E} + \mathbf{j} \times \mathbf{B} \right] - \gamma \mathbf{j}, \tag{7}$$

where we have added a phenomenological term $-\gamma \mathbf{j}$ to describe the current decay due to Coulomb scattering. The Lorentz force describes a change in momentum due to an applied force. The first term on the right-hand side, resulting from the convective derivative, describes an increase or decrease of momentum simply due to an accumulation or depletion of electrons at a certain spatial point.

Equations (6) and (7) have to be coupled to Maxwell's equations. The final full set of equations to be solved by a numerical scheme read as

$$\frac{\partial \mathbf{B}}{\partial t} = -\nabla \times \mathbf{E}, \tag{8}$$

$$\frac{\partial \mathbf{E}}{\partial t} = c^2 \nabla \times \mathbf{B} - \frac{1}{\epsilon_0} \mathbf{j}, \tag{9}$$

$$\frac{\partial \mathbf{j}}{\partial t} = \frac{e^2 n_0}{m_e} \mathbf{E} - \gamma \mathbf{j} + \sum_k \frac{\partial}{\partial r_k} \left(\frac{\mathbf{j} j_k}{e n_0 - \rho} \right) - \frac{e}{m_e} \left[\rho \mathbf{E} + \mathbf{j} \times \mathbf{B} \right], \tag{10}$$

where the charge density ρ has to be viewed as a function of the electric field since each occurrence of ρ can be replaced by the relation

$$\rho = \epsilon_0 \nabla \cdot \mathbf{E}. \tag{11}$$

This set of equations couples the dynamics of the EM field to the dynamics of the carriers described by their current density $\mathbf{j}$. It should be mentioned that Equation (10) contains rich physics. The first two terms represent the linear collective oscillation of the electrons with respect to the background ionic density $n_0(\mathbf{r})$, and the last two terms introduce three distinct sources for nonlinearities of the plasma. The second and third source are the well-known electric- and magnetic-component of the Lorentz force, respectively. The first source term is a generalized divergence originating from the convective time derivative of the electron velocity field $\mathbf{u}_e$ mentioned above.

III. PERTURBATIVE EXPANSION OF NONLINEARITIES

In order to obtain a simplified set of equations more suitable for a numerical approach we expand every quantity in a power series of the peak electric-field amplitude $|E_{\mathrm{exc}}|$ of the excitation pulse. Formally, we can write

$$\mathbf{E}(\mathbf{r},t) = \sum_j \mathbf{E}^{(j)}(\mathbf{r},t), \tag{12}$$

$$\mathbf{B}(\mathbf{r},t) = \sum_j \mathbf{B}^{(j)}(\mathbf{r},t), \tag{13}$$

$$\mathbf{j}(\mathbf{r},t) = \sum_j \mathbf{j}^{(j)}(\mathbf{r},t), \tag{14}$$

where the functions $\mathbf{E}^{(j)}$, $\mathbf{B}^{(j)}$, and $\mathbf{j}^{(j)}$ scale like $|E_{\mathrm{exc}}|^j$. A similar expansion automatically holds for the charge density by inserting Eq.(12) into Eq.(11)

$$\rho(\mathbf{r},t) = \epsilon_0 \sum_j \nabla \cdot \mathbf{E}^{(j)}(\mathbf{r},t). \tag{15}$$

Separating different orders, we obtain the linear response of the metal via

$$\frac{\partial \mathbf{B}^{(1)}}{\partial t} = -\nabla \times \mathbf{E}^{(1)}, \tag{16}$$

$$\frac{\partial \mathbf{E}^{(1)}}{\partial t} = c^2 \nabla \times \mathbf{B}^{(1)} - \frac{1}{\epsilon_0}\mathbf{j}^{(1)}, \tag{17}$$

$$\frac{\partial \mathbf{j}^{(1)}}{\partial t} = -\gamma \mathbf{j}^{(1)} + \frac{e^2 n_0}{m_e}\mathbf{E}^{(1)}. \tag{18}$$

This is equivalent to the well-known Drude model of a metal whose bulk plasma frequency $\omega_p^2 = e^2 n_0/m_e\epsilon_0$, as can be easily seen by Fourier transformation [56].

The second-order fields describe the lowest-order nonlinearity of the metal and are given by

$$\frac{\partial \mathbf{B}^{(2)}}{\partial t} = -\nabla \times \mathbf{E}^{(2)}, \tag{19}$$

$$\frac{\partial \mathbf{E}^{(2)}}{\partial t} = c^2 \nabla \times \mathbf{B}^{(2)} - \frac{1}{\epsilon_0}\mathbf{j}^{(2)}, \tag{20}$$

$$\frac{\partial \mathbf{j}^{(2)}}{\partial t} = -\gamma \mathbf{j}^{(2)} + \frac{e^2 n_0}{m_e}\mathbf{E}^{(2)} + \mathbf{S}^{(2)}, \tag{21}$$

together with the nonlinear source term

$$\mathbf{S}^{(2)} = \sum_k \frac{\partial}{\partial r_k}\left(\frac{\mathbf{j}^{(1)} j_k^{(1)}}{e n_0}\right) - \frac{e}{m_e}\left[\epsilon_0 \left(\nabla \cdot \mathbf{E}^{(1)}\right)\mathbf{E}^{(1)} + \mathbf{j}^{(1)} \times \mathbf{B}^{(1)}\right], \tag{22}$$

where k represents x, y and z coordinate. The homogeneous part of this set of equations is identical to the first-order equations such that the propagation of the SH field is modified by the Drude response of the metal. The source term

is expressed fully in terms of the first-order fields such that the sets of Eqs. (16)–(18) and (19)–(22) can be solved separately.

We want to stress that no approximations have been done yet except the expansion in orders of the exciting electric field. All fields are real quantities and no expansion in terms of "phase factor times slowly varying envelop" (see the Appendix) has been done so far. In principle, these equations can be numerically solved, and a switch-off analysis can be further utilized to distinguish the contribution of three nonlinear sources.

A three-dimensional finite-difference time-domain (FDTD) algorithm is employed to numerically solve the first-order and second-order equations separately [54]. Yee's discretization scheme is employed so that all field variables are defined in a cubic grid. Electric and magnetic fields are temporally separated by half a time step, they are also spatially interlaced by half a grid cell. Central differences in both space and time are then applied to Eqs. (16)–(22) [55]. In addition, all the NPs studied are made of gold with Drude-type permittivity approximated as

$$\epsilon(\omega) = 1.0 - \frac{\omega_p^2}{\omega(\omega + i\gamma)} \tag{23}$$

with the bulk plasma frequency $\omega_p = 1.367 \times 10^{16} s^{-1}$ and the phenomenological collision frequency $\gamma = 6.478 \times 10^{13} s^{-1}$ [34, 42, 57] (please notice that we employ ω_p, not n_0, in the simulations). In order to describe the energy conversion efficiency in the nonlinear-optical process, we define a normalized SH intensity,

$$\eta = |\mathbf{E}^{(2)}(2\omega_0)/\mathbf{E}^{(1)}(\omega_0)|^2, \tag{24}$$

to measure the strength of the far-field SH signal, where ω_0 is the frequency of the incident fundamental-frequency (FF) wave.

Our interests in the present article are limited to arrays of metallic NPs (also named as planar metamaterial [34, 40, 44]) with normal incidence, the computational domain is therefore arranged as follows: an array of NPs is placed in the middle of the space with its top and bottom surfaces positioned perpendicular to the z direction; plane waves propagating along the z axis are generated by a total field/scattering field technique [54]; perfect matched absorbing boundary conditions are applied at the top and bottom of the computational space together with periodic boundary conditions on other boundaries [58]; the structure studied extends periodically in the x and y directions, and only single unit cell is needed in the computational space. In addition, in all the following simulations, the size of the spatial grid cell is fixed as 2.5 nm, and the associate time step is 4.17 attosecond.

IV. THEORY-EXPERIMENT COMPARISON

In this section detailed comparisons between the numerical evaluations of our theory with the experiments done in two independent laboratories are presented [34, 39, 40, 42]. First, we consider a series of experiments reported in Refs.[34, 40, 42], in which NPs with different geometrical configurations are studied (see Fig. 1). Among them the U-shaped NPs (split-ring resonators) are known to possess negative effective permeabilities in certain frequency regions and are generally referred to as magnetic metamaterials [34, 59, 60, 61, 62]. Strictly speaking, those "metamaterials" are only the first step towards a true three-dimensional bulk material. So far, most of the metamaterials are rather two-dimensional arrays of unit cells to study the fundamental properties of the NPs. These samples are supported by infinite-thickness glass (with $\epsilon = 2.25$) substrate coated with a thin film of indium-tin-oxide (with $\epsilon = 3.8$), and the thicknesses of the gold and indium-tin-oxide layers are 25 nm and 5 nm, respectively [34, 40, 42]. It should be emphasized that the geometrical parameters of these NPs are chosen such that each structure has a resonance around 1500-nm wavelength.

Our theoretical results are summarized in Fig. 1. We note that the simulations qualitatively agree with the corresponding experimental measurements. The SH signal strength emitted from the U-shape particles with x-polarized FF incidence is found as 6.6×10^{-11} from the simulation, which is quite close to the experimental result of 2.0×10^{-11} [40] (Please notice that the SH strength reported in Ref.[40] has been corrected in the sequent erratum). Our simulation thus reproduces the strength of the experimental SH signal. The following important conclusions can be further extracted from Fig. 1:

(1) The polarization state of the far-field SH signal is always y-polarized (Fig. 2) for both x- or y-polarized incident fields (except the rectangle-shaped NPs). There thus exists a universal selection rule, that is, a mirror symmetry of the metallic NPs in one direction completely prohibits a polarization component of SHG in that direction. This symmetry dependence can be explained as follows. Within the electric dipole approximation, the far-field SH electric field can be related to the incident FF field such that [50, 52]

$$\mathbf{E}(2\omega) = \overleftrightarrow{\chi}^{(2)} \cdot \mathbf{E}(\omega)\mathbf{E}(\omega), \tag{25}$$

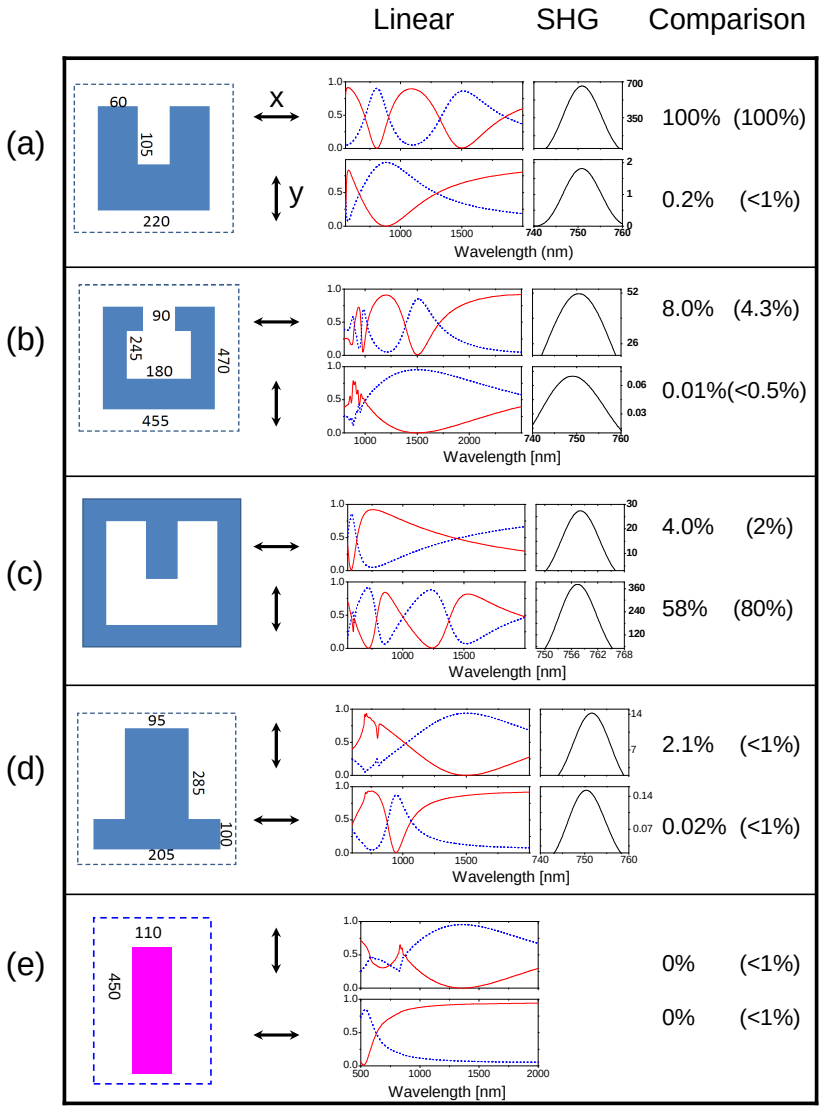

FIG. 1: (Color online) Comparisons of numerical simulations and experiments for different arrays of gold nanoparticles. The different columns (from left to right) show shape of nanoparticles, the polarization of the incident light (indicated by the arrows), the linear transmission (solid) and reflection (dashed) spectra, theoretical SHG spectra (amplified 13 orders of magnitude), the relative strengths obtained by the theory and the corresponding experiments (inside brackets). For all the structures, the polarization of the generated second-harmonic waves are along the y direction. The illuminating fundamental-frequency wave has wavelength around 1500 nm and amplitude of 2×10^7 (V/m). (a) The U-shape particle corresponds to the experimental sample shown in Fig.(1A) of Ref.[34] (also at Fig.(1a) of Ref.[40]), with lattice constant $a_x = a_y$ =305 nm. (b) The C-shape particle corresponds to the experimental sample shown in Fig.(1C) of Ref.[34] (also at Fig.(1c) of Ref.[40]), with a_x = 567.5 nm and a_y = 590 nm. (c) The inverse-U-shape particle corresponds to the experimental sample shown in Ref.[42], with $a_x = a_y$ =305 nm. (d) The T-shape particle corresponds to the experimental sample shown in Fig.(2c) of Ref.[40], with a_x = 295 nm and a_y = 465 nm. (e) The rectangle-shape corresponds to the experimental sample shown in Fig.(2b) of Ref.[40]. Here a_x and a_y are the lattice constants along x and y direction, respectively. All nanoparticles dimensions shown are in nanometer.

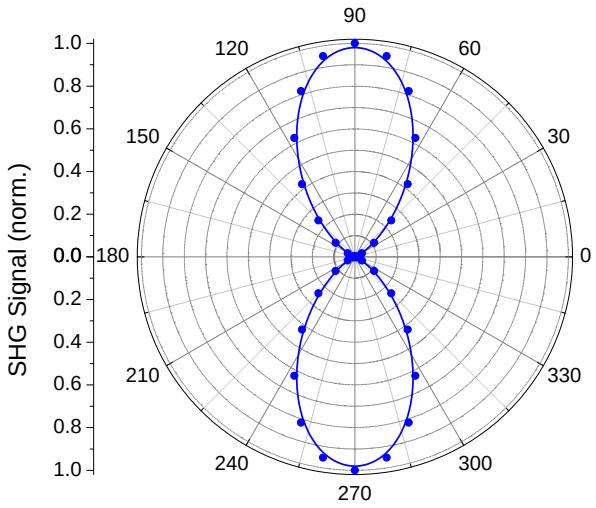

FIG. 2: (Color online) The polarization state of the second harmonic emission from an array of U-shape particles illuminated with a x-polarized plane wave at the fundamental frequency. The second-harmonic signal is a function of the measuring angle (not the polarization of the incident field) θ ($\theta = 0$ corresponds to the x direction). The corresponding experiment measurement is shown in Fig.(2B) of Ref.[34].

where $\overleftrightarrow{\chi}^{(2)}$ stands for a generalized dyadic second-order nonlinear susceptibility. The x-coordinate mirror symmetry results in the following vanishing elements, $\chi^{(2)}_{xxx}$, $\chi^{(2)}_{xyy}$, $\chi^{(2)}_{yxy}$ and $\chi^{(2)}_{yyx}$. Further representing the FF field as $\mathbf{E}(z,\omega) = E_0 e^{i(\omega t - kz)} [\cos\theta \mathbf{e}_x + \sin\theta \mathbf{e}_y]$, with $k = \omega/c$ being the wave number, θ being the polarization angle and $\mathbf{e}_x$ ($\mathbf{e}_y$) being the unit vector along the x (y) direction, we obtain

$$\begin{aligned} E_x(2\omega) &= E_0^2 \chi^{(2)}_{xxy} \sin 2\theta, \\ E_y(2\omega) &= E_0^2 \left[\chi^{(2)}_{yxx} \cos^2\theta + \chi^{(2)}_{yyy} \sin^2\theta \right]. \end{aligned} \tag{26}$$

The $E_x(2\omega)$ component is simply proportional to $\sin 2\theta$, and therefore vanishes for $\theta = 0$ or $\theta = \pi/2$, corresponding to x- or y-polarized FF incidence. On the other hand, the relationship between $E_y(2\omega)$ and θ is nontrivial, and it survives for $\theta = 0$ and $\theta = \pi/2$.

(2) Similar to the fact that SHG at metal surfaces can be significantly enhanced by coupling incident light into surface polariton resonances [8], the presence of structural plasmonic resonances also can greatly enhance SHG from metallic NPs. Moreover, different-order plasmonic resonances make different contributions to the SHG. For example, an enlarged version of the U-shape NP from Fig.(1a) possesses a second-order resonance coincident with the fundamental resonance of the original. The SHG emitting from the fundamental resonance of the original U is considerably stronger than the SHG from the second-order resonance of the larger structure, even without the perfect phase matching requirement, because the near field enhancement is maximized for the fundamental resonance [25, 53, 63, 64].

(3) It is found in the simulation that no SH signal is emitted from the rectangle-shaped NPs in the far field. As stated earlier, this is a direct consequence of the fact that an individual rectangle-shaped NP possesses mirror symmetries along both x and y directions. A dipole SH source is therefore forbidden and only quadrupole sources (and higher-order multipoles) are allowed (the retardation effects are negligible here since the thicknesses of NPs are much smaller than the SH wavelength, while these effects are found to excite nonlocal SH dipole for large-size gold nanospheres [31]). For a periodic array of rectangle-shaped NPs with translational symmetry, the SH signal from each individual NP interfere destructively. Therefore, only near-field SH signal exists for the array. However, slight far-field SH signal is observed in the experiment. This deviation is believed to originate from the fact that the samples are not rigorously inversion-symmetry because of the fabrication imperfections (see the scanning electron micrograph shown in Ref.[40]).

Next we study the effect of the gap on the far-field SH strength in noncentrosymmetric T-shaped gold nanodimers (Fig. 3). The corresponding experiment is reported in Ref.[39], and the scanning electron micrograph images of two dimers are shown in Fig. 3. Obviously, these T-shaped dimers does not possess any mirror symmetry along either x or y direction. The gold array is 20 nm thick, with a lattice spacing of 400 nm. It is further covered with a 20-nm protective layer of glass and supported with an infinite-thickness glass substrate.

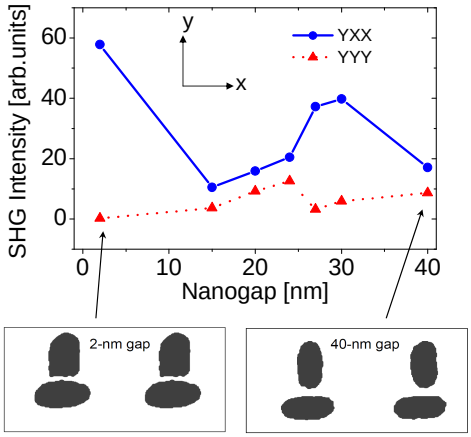

FIG. 3: (Color online) Second harmonic generation in noncentrosymmetric nanodimers with varying gaps. The configuration such as YXX indicates y-polarized second-harmonic signal with x-polarized fundamental field. The two images show the unit cells as simulated, containing two structures which were digitized from the scanning electron micrograph images of the experimental samples (Ref.[39]). The corresponding experimental results are reported in Ref.[39] (Fig.1 and Fig.3).

To include the relative difference between the configurations of the samples, the NPs (for all gaps) employed in our simulations are obtained by directly scanning the experimental samples, and the computational cell consists of two T-shaped dimers. Our numerical results are plotted in Fig. 3 and reproduce the experimental observations qualitatively. More specifically, the SHG for two configurations, YXX (y-polarized SH signal with x-polarized fundamental fields) and YYY (y-polarized SH signal with y-polarized fundamental fields), strongly depend on the size of the gap, in a non-monotonically decreasing fashion. The 40-nm gap yields weak SHG responses for both configurations and the largest SHG response occurs for YXX from the 2-nm gap. For gaps smaller than 15 nm, the YYY response is much weaker than the YXX response. On the other hand in a simulation of ideal structures, without the geometrical variation of the dimers induced by the fabrication imperfections, the YXX response decreases monotonically with increasing gap. The non-monotonic responses observed in the experiments thus arise from two sources, the near-field enhancement around the NPs decreases with increasing the gap, and variations of the overall shape of different-gap nanodimers due to the fabrication imperfections.

V. DISCUSSION AND CONCLUSIONS

The experiment-theory agreement presented above suggests that, in contrast to an ideally infinite interface whose SH response strongly localizes in its surface region, the overall shape of the NP plays an important or even dominant role in determining efficient SH emission [48]. Hence, even without an accurate description of the surface electrons, our classical model can not only successfully reproduce the experimental observations qualitatively, but also reproduce the SH intensities.

It should be mentioned that Schaich developed an approach quite similar to ours to study SHG by periodically-structured metal surfaces [65]. The major difference is that analytical parametrizations of SHG at the (top) interface of a thick metal slab [24, 66, 67, 68] are taken by assuming the parametrization scheme still works even when the flat metal surfaces are not of infinite extent but have edges and corners. However, the validation of this assumption is unclear, especially for subwavelength objects where the separation between two neighboring edges may only be tens of nanometers and rapid variations of the parametrizations are therefore expected. Furthermore, this parametrization scheme limits the application of his approach for NP with complicated boundaries such as the nanodimers studied above as well as NPs with thin thicknesses. In addition, there are some generalized theoretical works regarding nonlinear metamaterials [69, 70] and the nonlinear properties of negative-index metamaterials [71, 72].

We want to point out that our classical model contains only the influence of the conduction electrons and neglects contributions from other sources such as core electrons and lattice phonons. It therefore, for example, cannot correctly describe third-order nonlinearities where the electronic polarization is negligible comparing with other effects such as

saturated atomic absorption [52]. To include the third-order nonlinearities, we need to add another current term

$$\mathbf{j}_{\mathrm{c}}(t) = \chi^{(3)} \frac{d}{dt} |\mathbf{E}|^2 \mathbf{E}, \tag{27}$$

where $\chi^{(3)}$ is the third-order nonlinear susceptibility, which equals $7.56 \times 10^{-19} \mathrm{m}^2/\mathrm{V}^2$ for gold [53]. The new set of equations has been utilized to study third-harmonic generation from the NPs reported in Ref.[40]. It was demonstrated (see Appendix II) that our simulations not only reproduce the overall strength of the experimentally observed third harmonic signals, but also qualitatively reproduce the structure dependent changes. As expected, we found the third harmonic strength to be closely related to the localization degree of the FF field inside the metal.

In conclusion, a classical theory of second-harmonic generation from metallic nanoparticles is presented. The conductor-band electrons inside the metal are approximated as a classical continuous plasmonic fluid, and its dynamics under an external electromagnetic field are described by the plasma wave equations self-consistently. A three-dimensional finite-difference time-domain approach is further applied to solve these equations numerically. By comparing theoretical results directly with the corresponding experiments, it is demonstrated that our classical theory, even without an accurate treatment of the surface electrons, qualitatively captures the dominant physical mechanisms of second-harmonic generations from metallic nanoparticles. This agreement suggests that the second-harmonic emission from nanoparticles depends strongly on their overall configurations.

VI. ACKNOWLEDGMENT

The authors are grateful to Prof. Martti Kauranen at the Tampere University for providing the SEM images of the experimental samples. They also want to thank Prof. Martin Wegener and his group at the Universität Karlsruhe, Dr. Jens Förstner at the Paderborn University, Prof. Moysey Brio, Dr. Miroslav Kolesik and Dr. Colm Dineen at the University of Arizona for their invaluable discussions. This work is supported by the Air Force Office of Scientific Research (AFOSR), under Grant No. FA9550-07-1-0010 and FA9550-04-1-0213. J. V. Moloney acknowledges support from the Alexander von Humboldt foundation.

VII. APPENDIX I: APPROXIMATION FOR QUASI-MONOCHROMATIC EXCITATION

For a quasi-monochromatic pulse with central angular frequency ω_0, one can classify the different contributions in terms of their complex phase factor. For example, the linear electric field is given by

$$\mathbf{E}^{(1)}(\mathbf{r},t) = \left[\widetilde{\mathbf{E}}^{(1)}(\mathbf{r},t)\mathrm{e}^{-i\omega_0 t} + \mathrm{c.c.}\right] \tag{28}$$

with the slowly varying complex field $\widetilde{\mathbf{E}}^{(1)}$, while the second order field

$$\mathbf{E}^{(2)}(\mathbf{r},t) = \widetilde{\mathbf{E}}_0^{(2)}(\mathbf{r},t) + \left[\widetilde{\mathbf{E}}_2^{(2)}(\mathbf{r},t)\mathrm{e}^{-i2\omega_0 t} + \mathrm{c.c.}\right] \tag{29}$$

has a second-harmonic contribution proportional to the phase factor $\mathrm{e}^{-i2\omega_0 t}$ multiplied with the slowly varying complex amplitude $\widetilde{\mathbf{E}}_2^{(2)}$, as well as a slowly varying low-frequency part $\widetilde{\mathbf{E}}_0^{(2)}$. The magnetic field and the current can be expanded in a similar way.

As a next step, we want to express the source term from Eq. (22) solely in terms of the linear electric field. To that aim, we use the linear Eqs. (16) and (18) with the quasi-monochromatic approximation of Eq. (28) and obtain

$$i\omega_0 \widetilde{\mathbf{B}}^{(1)} = \nabla \times \widetilde{\mathbf{E}}^{(1)} \quad \Longrightarrow \quad \widetilde{\mathbf{B}}^{(1)} = -\frac{i}{\omega_0} \nabla \times \widetilde{\mathbf{E}}^{(1)}, \tag{30}$$

$$-i\omega_0 \widetilde{\mathbf{j}}^{(1)} = -\gamma \widetilde{\mathbf{j}}^{(1)} + \frac{e^2 n_0}{m_e} \widetilde{\mathbf{E}}^{(1)} \quad \Longrightarrow \quad \widetilde{\mathbf{j}}^{(1)} = \frac{i}{\omega_0 + i\gamma} \frac{e^2 n_0}{m_e} \widetilde{\mathbf{E}}^{(1)}, \tag{31}$$

where we have matched the terms with equal phase factor $\mathrm{e}^{-i\omega_0 t}$.

Since every contribution to $\mathbf{S}^{(2)}$ in Eq. (22) is of the form of a product $A^{(1)}B^{(1)}$ between two first order terms, these products according Eq. (28) can be expressed as

$$\begin{aligned} A^{(1)}B^{(1)} &= \left(\widetilde{A}^{(1)} \exp^{-i\omega_0 t} + \mathrm{c.c.}\right)\left(\widetilde{B}^{(1)} \exp^{-i\omega_0 t} + \mathrm{c.c.}\right) \\ &= \left[\widetilde{A}^{(1)}\widetilde{B}^{(1)} \exp^{-i2\omega_0 t} + \mathrm{c.c.}\right] + \left[\widetilde{A}^{(1)}(\widetilde{B}^{(1)})^* + \mathrm{c.c.}\right]. \end{aligned} \tag{32}$$

Thus, for the SH source $\widetilde{\mathbf{S}}_2^{(2)}$, only the products of the slowly varying complex fields have to be calculated. They can be computed term by term and in the limit $\gamma = 0$ the first contribution from the convective term is given by

$$\widetilde{\mathbf{S}}_2^{(2)}\Big|_{\text{conv}} = \sum_k \frac{\partial}{\partial r_k}\frac{\widetilde{\mathbf{j}}_1\widetilde{j}_{1,k}}{en_0} = -\frac{e}{m_e}\frac{\epsilon_0}{\omega_0^2}\left[(\omega_{\text{pl}}^2\widetilde{\mathbf{E}}^{(1)}\cdot\nabla)\widetilde{\mathbf{E}}^{(1)} + \widetilde{\mathbf{E}}^{(1)}\left(\nabla\cdot(\omega_{\text{pl}}^2\widetilde{\mathbf{E}}^{(1)})\right)\right], \tag{33}$$

where the plasma frequency is defined as $\omega_{\text{pl}}^2(\mathbf{r}) = e^2 n_0(\mathbf{r})/(m_e\epsilon_0)$. The second term of Eq. (22) – the electric Lorentz force – is already expressed solely in terms of the electric field and the third, magnetic term can be written as

$$\widetilde{\mathbf{S}}_2^{(2)}\Big|_{\text{magn}} = -\frac{e}{m_e}\widetilde{\mathbf{j}}^{(1)}\times\widetilde{\mathbf{B}}^{(1)} = \frac{e}{m_e}\frac{\epsilon_0}{\omega_0^2}\omega_{\text{pl}}^2\left[(\widetilde{\mathbf{E}}^{(1)}\cdot\nabla)\widetilde{\mathbf{E}}^{(1)} - \frac{1}{2}\nabla\left(\widetilde{\mathbf{E}}^{(1)}\cdot\widetilde{\mathbf{E}}^{(1)}\right)\right]. \tag{34}$$

Adding up all three contributions to the complex SH source term $\widetilde{\mathbf{S}}_2^{(2)}$ is then given by

$$\widetilde{\mathbf{S}}_2^{(2)} = -\frac{e}{m_e}\frac{\epsilon_0}{\omega_0^2}\left[\widetilde{\mathbf{E}}^{(1)}\left(\nabla\cdot(\omega_{\text{pl}}^2\widetilde{\mathbf{E}}^{(1)})\right) + \omega_0^2\widetilde{\mathbf{E}}^{(1)}\left(\nabla\cdot\widetilde{\mathbf{E}}^{(1)}\right) + \frac{\omega_{\text{pl}}^2}{2}\nabla\left(\widetilde{\mathbf{E}}^{(1)}\cdot\widetilde{\mathbf{E}}^{(1)}\right)\right]. \tag{35}$$

Furthermore, from the first order wave equation, we find that

$$\nabla\cdot\widetilde{\mathbf{E}}^{(1)} = \frac{1}{\omega_0^2}\nabla\cdot(\omega_{\text{pl}}^2\widetilde{\mathbf{E}}^{(1)}), \tag{36}$$

such that the SH source can be accordingly simplified to

$$\widetilde{\mathbf{S}}_2^{(2)} = -\frac{e\,\epsilon_0}{m_e}\left[2\widetilde{\mathbf{E}}^{(1)}\left(\nabla\cdot\widetilde{\mathbf{E}}^{(1)}\right) + \frac{1}{2}\frac{\omega_{\text{pl}}^2}{\omega_0^2}\nabla\left(\widetilde{\mathbf{E}}^{(1)}\cdot\widetilde{\mathbf{E}}^{(1)}\right)\right]. \tag{37}$$

In a similar fashion, also the low-frequency source $\widetilde{\mathbf{S}}_0^{(2)}$ can be derived. Repeating analogous steps for the second term of Eq. (32) we obtain

$$\widetilde{\mathbf{S}}_0^{(2)} = \frac{e\,\epsilon_0}{m_e}\frac{\omega_{\text{pl}}^2}{\omega_0^2}\nabla|\widetilde{\mathbf{E}}^{(1)}|^2, \tag{38}$$

which is the well-known ponderomotive force.

In order to insert the nonlinear source into the differential equation for $\mathbf{j}^{(2)}$, Eq. (21), we have to express the total real source in terms of the slowly varying complex amplitudes,

$$\begin{aligned}\mathbf{S}^{(2)} &= \widetilde{\mathbf{S}}_0^{(2)} + \left[\widetilde{\mathbf{S}}_2^{(2)}\mathrm{e}^{-i2\omega_0 t} + \text{c.c.}\right] \\ &= \frac{e\,\epsilon_0}{m_e}\frac{\omega_{\text{pl}}^2}{\omega_0^2}\nabla|\widetilde{\mathbf{E}}^{(1)}|^2 - \frac{e\,\epsilon_0}{m_e}\left\{\left[2\widetilde{\mathbf{E}}^{(1)}\left(\nabla\cdot\widetilde{\mathbf{E}}^{(1)}\right) + \frac{1}{2}\frac{\omega_{\text{pl}}^2}{\omega_0^2}\nabla\left(\widetilde{\mathbf{E}}^{(1)}\cdot\widetilde{\mathbf{E}}^{(1)}\right)\right]\mathrm{e}^{-i2\omega_0 t} + \text{c.c.}\right\}.\end{aligned} \tag{39}$$

This result cannot be expressed by the real linear electric field for all frequencies. But since we are most interested in the second harmonic generation, we can approximate the source by

$$\mathbf{S}^{(2)}\Big|_{\text{SHG}} \approx -\frac{e\,\epsilon_0}{m_e}\left[2\mathbf{E}^{(1)}\left(\nabla\cdot\mathbf{E}^{(1)}\right) + \frac{1}{2}\frac{\omega_{\text{pl}}^2}{\omega_0^2}\nabla|\mathbf{E}^{(1)}|^2\right], \tag{40}$$

where $\mathbf{E}^{(1)}$ is again the full, fast oscillating, real-valued electric field obtained by the set of Eqs. (16)–(18). By inserting the expansion from Eq. (28) into Eq. (40) it can be easily shown that the second-harmonic contribution of Eq. (39) is exactly reproduced while the low-frequency contribution of Eq. (40) is different from that of Eq. (39).[74]

To numerically solve the $\mathbf{j}_2$ equation with the FDTD approach, Eqs. (19)–(21) with the source given by Eq. (40) have to be solved. Technically, the current is split into three different contributions according to

$$\frac{\partial\mathbf{j}_A^{(2)}}{\partial t} = -\gamma\mathbf{j}_A^{(2)} + \frac{e^2 n_0}{m_e}\mathbf{E}^{(2)}, \tag{41}$$

$$\frac{\partial\mathbf{j}_B^{(2)}}{\partial t} = -\gamma\mathbf{j}_B^{(2)} - 2\frac{e\,\epsilon_0}{m_e}\mathbf{E}^{(1)}\left(\nabla\cdot\mathbf{E}^{(1)}\right), \tag{42}$$

$$\frac{\partial\mathbf{j}_C^{(2)}}{\partial t} = -\gamma\mathbf{j}_C^{(2)} - \frac{e\,\epsilon_0}{m_e}\frac{1}{2}\frac{\omega_{\text{pl}}^2}{\omega_0^2}\nabla|\mathbf{E}^{(1)}|^2, \tag{43}$$

where the sum of $\mathbf{j} = \mathbf{j}_A + \mathbf{j}_B + \mathbf{j}_C$ defines the total current.

TABLE I: Third harmonic strength (10^{-12})

Structure	Experimental results	Numerical results
U-shaped (Fig.(1a))	3.0	1.14[b]
T-shaped (Fig.(1d))	0.66	0.80
Rectangle (Fig.(1e))	0.21	0.26

[a]The fundamental incidence is x-polarized.
[b]The difference between experiment and simulation is possibly due to experimental imperfections in the real structure, see the Fig.(2a) of Ref.[40].

VIII. APPENDIX II: NUMERICAL RESULTS OF THIRD-HARMONIC GENERATION

Third-harmonic generation from the samples described in Ref.[40] are numerically simulated, and the obtained results are listed in Table I. We see that our simulations reproduce the overall strength of the experimentally observed third-harmonic signals, and qualitative reproduce the structure dependent changes. As expected, we find the third-harmonic strength to be closely related to the localization degree of the fundamental field inside the metal. In addition, although the strength of second-harmonic and third-harmonic signals are comparable [73], almost negligible interactions are observed in our simulations. Second-harmonic generation and third-harmonic generation from metallic nanoparticles can be therefore studied separately.

[1] F. Brown, R. E. Parks, A. M. Sleeper, "Nonlinear Optical Reflection from a Metallic Boundary", Phys. Rev. Lett. 14, 1029 (1965).
[2] P. A. Franken, A. E. Hill, C. W. Peters, G. Weinreich, "Generation of Optical Harmonics", Phys. Rev. Lett. 7, 118 (1961).
[3] J. E. Sipe and G. I. Stegeman, *Surface Polaritons: Electromagnetic Waves at Surfaces and Interfaces*, edited by V. M. Agranovich and D. L. Mills (North-Holland, Amsterdam, 1982).
[4] D. Guidotti, T. A. Driscoll, H. J. Gerritsen, "Second harmonic generation in centro-symmetric semiconductors", Solid State Commun. 46, 337 (1983).
[5] J. E. Sipe, D. J. Moss, H. M. van Driel, "Phenomenological theory of optical second- and third-harmonic generation from cubic centrosymmetric crystals", Phys. Rev. B 35, 1129 (1987).
[6] C. K. Chen, A. R. B. de Castro, Y. R. Shen, "Surface-Enhanced Second-Harmonic Generation", Phys. Rev. Lett. 46, 145 (1981).
[7] C. K. Chen, T. F. Heinz, D. Ricard, Y. R. Shen, "Surface-enhanced second-harmonic generation and Raman scattering", Phys. Rev. B 27, 1965 (1983).
[8] S. Janz and H. M. van Driel, "Second-harmonic generation from metal surfaces," International J. Nonlinear Optical Phys. 2, 1(1993).
[9] S. S. Jha, "Theory of optical harmonic generation at a metal surface", Phys. Rev. 140, A2020 (1965).
[10] N. Bloembergen, R. K. Chang, S. S. Jha, C. H. Lee, "Optical second-harmoni generation in reflection from media with inverse symmetry", Phys. Rev. 174, 813 (1968).
[11] J. Rudnick, E. A. Stern, "Second-harmoni radiation from metal surfaces", Phys. Rev. B 4, 4272 (1971).
[12] A. Eguiluz, J. J. Quinn, "Hydrodynamic model for surface plasmons in metals and degenerate semiconductors", Phys. Rev. B 14, 1347 (1976).
[13] J. E. Sipe, V. C. Y. So, M. Fukui, G. I. Stegeman, "Analysis of second-harmonic generation at metal surfaces", Phys. Rev. B 21, 4389 (1980).
[14] X. M. Hua, J. I. Gersten, "Theory of second-harmonic generation by small metal spheres", Phys. Rev. B 33, 3756 (1986).
[15] J. A. Maytorena, W. Luis Mochán, B. S. Mendoza, "Hydrodynamic model for sum and difference frequency generation at metal surfaces", Phys. Rev. B 57, 2580 (1998).
[16] P. Guyot-Sionnest, W. Chen, Y. R. Shen, "General considerations on optical second-harmonic generation from surfaces and interfaces", Phys. Rev. B 33, 8254 (1986).
[17] J. I. Dadap, J. Shan, K. B. Eisenthal, T. F. Heinz, "Second-Harmonic Rayleigh Scattering from a Sphere of Centrosymmetric Material", Phys. Rev. Lett. 83, 4045 (1999).
[18] M. I. Stockman, D. J. Bergman, C. Anceau, S. Brasselet, J. Zyss, "Enhanced Second-Harmonic Generation by Metal Surfaces with Nanoscale Roughness: Nanoscale Dephasing, Depolarization, and Correlations", Phys. Rev. Lett. 92, 057402 (2004).
[19] J. I. Dadap, J. Shan, T. F. Heinz, "Theory of optical second-harmonic generation from a Sphere of Centrosymmetric Material: small-particle limit", J. Opt. Soc. Am. B 21, 1328 (2004).
[20] K. Li, M. I. Stockman, D. J. Bergman, "Enhanced second harmonic generation in a self-similar chain of metal nanospheres",

Phys. Rev. B 72, 153401 (2005).
[21] L. Cao, N. C. Panoiu, R. M. Osgood, "Surface second-harmonic generation from surface plasmon waves scattered by metallic nanostructures", Phys. Rev. B 75, 205401 (2007).
[22] G. Bachelier, I. Russier-Antoine, E. Benichou, C. Jonin, P. F. Brevet, "Multipolar second-harmonic generation in noble metal nanoparticles," J. Opt. Soc. Am. B 25, 955 (2008).
[23] T. F. Heinz, in *Nonlinear surface electromagnetic phenomena*, edited by H. Ponath and G. Stegeman (Elsevier, Amsterdam, 1991).
[24] A. Liebsch, *Electronic Excitations at Metal Surfaces* (Plenum press, 1997).
[25] J. B. Pendry, A. J. Holden, D. J. Robbins, W. J. Stewart, "Magnetism from conductors and enhanced nonlinear phenomena", IEEE Trans. Microwave Theory Tech. 47, 2075 (1999).
[26] Steven A. Maier, *plasmonic: fundamental and applications* (Springer, 2007).
[27] C. Anceau, S. Brasselet, J. Zyss, P. Gadenne, "Local second-harmonic generation enhancement on gold nanostructures probed by two-photon microscopy", Opt. Lett. 28, 713 (2003).
[28] A. Bouhelier, M. Beversluis, A. Hartschuh, and L. Novotny, "Near-Field Second-Harmonic Generation Induced by Local Field Enhancement", Phys. Rev. Lett. 90, 013903 (2003).
[29] A. Nahata, R. A. Linke, T. Ishi, K. Ohashi, "Enhanced nonlinear optical conversion from a periodically nanostructured metal film", Opt. Lett. 28, 423 (2003).
[30] D. Krause, C. W. Teplin, C. T. Rogers, "Optical surface second harmonic measurements of isotropic thin-film metals: Gold, silver, copper, aluminum, and tantalum", J. Appl. Phys. 96, 3626 (2004).
[31] J. Nappa, G. Revillod, I. Russier-Antoine, E. Benichou, C. Jonin, P. F. Brevet, "Electric dipole origin of the second harmonic generation of small metallic particles", Phys. Reb. B 71, 165407 (2005).
[32] C. C. Neacsu, G. A. Reider, M. B. Raschke, "Second-harmonic generation from nanoscopic metal tips: Symmetry selection rules for single asymmetric nanostructures", Phys. Rev. B 71, 201402(R) (2005).
[33] M. D. McMahon, R. Lopez, R. F. Haglund, E. A. Ray, P. H. Bunton, "Second-harmonic generation from arrays of symmetric gold nanoparticles", Phys. Rev. B 73, 041401(R) (2006).
[34] M. W. Klein, C. Enkrich, M. Wegener, S. Linden, "Second-Harmonic Generation from Magnetic Metamaterials", Science 313, 502 (2006).
[35] J. Shan, J. I. Dadap, I. Stiopkin, G. A. Reider, T. F. Heinz, "Experimental study of optical second-harmonic scattering from spherical nanoparticles", Phys. Rev. A 73, 023819 (2006).
[36] S. Abe, K. Kajikawa, "Linear and nonlinear optical properties of gold nanospheres immobilized on a metallic surface", Phys. Rev. B 74, 035416 (2006).
[37] J. A. H. van Nieuwstadt, M. Sandtke, R. H. Harmsen, F. B. Segerink, J. C. Prangsma, S. Enoch, L. Kuipers, "Strong Modification of the Nonlinear Optical Response of Metallic Subwavelength Hole Arrays", Phys. Rev. Lett. 97, 146102 (2006).
[38] S. Kujala, B. K. Canfield, M. Kauranen, Y. Svirko, J. Turunen, "Multipole Interference in the Second-Harmonic Optical Radiation from Gold Nanoparticles", Phys. Rev. Lett. 98, 167403 (2007).
[39] B. K. Canfield, H. Husu, J. Laukkanen, B. Bai, M. Kuittinen, J. Turunen, M. Kauranen, "Local field asymmetry drives second-harmonic generation in noncentrosymmetric nanodimers", Nano Lett. 7, 1251 (2007).
[40] M. W. Klein, M. Wegener, N. Feth, S. Linden, "Experiments on second- and third-harmonic generation from magnetic metamaterials", Opt. Express 15, 5238 (2007). Also the erratum at Opt. Express 16, 8055 (2008).
[41] M. C. Larciprete, A. Belardini, M. G. Cappeddu, D. de Ceglia, M. Centini, E. Fazio, C. Sibilia, M. J. Bloemer, and M. Scalora, "Second-harmonic generation from metallodielectric multilayer photonic-band-gap structures", Phys. Rev. A 77, 013809 (2008).
[42] N. Feth, S. Linden, M. W. Klein, M. Decker, F. Niesler, Y. Zeng, W. Hoyer, J. Liu, S. W. Koch, J. V. Moloney, and M. Wegener, "Second-harmonic generation from complementary split-ring resonators", Opt. Lett. 33, 1975 (2008).
[43] S. Kujala, B. K. Canfield, M. Kauranen, Y. Svirko, J. Turunen, "Multipolar analysis of second-harmonic radiation from gold nanoparticles", Opt. Express, 16, 17196 (2008).
[44] E. Kim, F. Wang, W. Wu, Z. Yu, Y. R. Shen, "Nonlinear optical spectroscopy of photonic metamaterials", Phys. Rev. B 78, 113102 (2008).
[45] Y. Maeda, T. Iwai, Y. Satake, K. Fujii, S. Miyatake, D. Miyazaki, G. Mizutani, "Optical second-harmonic spectroscopy of Au(887) and Au(443) surfaces", Phys. Rev. B 78, 075440 (2008).
[46] H. Husu, B. K. Canfield, J. Laukkanen, B. Bai, M. Kuittinen, J. Turunen, M. Kauranen, "Chiral coupling in gold nanodimers", Appl. Phys. Lett. 93, 183115 (2008).
[47] M. Zavelani-Rossi, M. Celebrano, P. Biagioni, D. Polli, M. Finazzi, L. Duò, G. Cerullo, M. Labardi, M. Allegrini, J. Grand, P.-M. Adam, "Near-field second-harmonic generation in single gold nanoparticles", Appl. Phys. Lett. 92, 093119 (2008).
[48] M. Finazzi, P. Biagioni, M. Celebrano, L. Duò, "Selection rules for second-harmonic generation in nanoparticles", Phys. Rev. B 76, 125414 (2007).
[49] W. Hoyer, M. Kira and S. W. Koch, in *Classical and quantum optics of semiconductor nanostructures* (Springer, 2008).
[50] T. J. M. Boyd, J. J. Sanderson, *The physics of plasmas* (Cambridge, 2003).
[51] J. Freidberg, *Plasma Physics and Fusion Energy* (Cambridge, 2007).
[52] Y. R. Shen, *The principles of Nonlinear Optics* (John Wiley & Sons, New York, 1984).
[53] R. W. Boyd, *Nonlinear Optics* (Second edition, Academic press, 2003).
[54] A. Taflove and S. C. Hagness, *Computational Electrodynamics: the finite-difference time-domain method* (Second Edition, Artech House, Boston, 2000).

[55] K. Yee, "Numerical solution of initial boundary value problems involving Maxwell's equations in isotropic media", IEEE Trans. Antennas and Propagat., 14, 302 (1996).
[56] M. Born and E. Wolf, *Principle of Optics* (Seven Edition, Cambridge, 1999).
[57] E. D. Palik, *Handbook of optical constants of solids* (Academic, Orlando, 1985).
[58] J. P. Berenger, "A perfectly matched layer for the absorption of electromagnetic waves", J. Computational Physics, 114, 185-200 (1994).
[59] C. Rockstuhl, F. Lederer, C. Etrich, Th. Zentgraf, J. Kuhl, and H. Giessen, "On the reinterpretation of resonances in split-ring-resonators at normal incidence", Opt. Express 14, 8827 (2006).
[60] N. Lazarides, M. Eleftheriou, G. P. Tsironis, "Discrete Breathers in Nonlinear Magnetic Metamaterials", Phys. Rev. Lett. 97, 157406 (2006).
[61] D. R. Smith, W. J. Padilla, D. C. Vier, S. C. Nemat-Nasser, S. Schultz, "Composite Medium with Simultaneously Negative Permeability and Permittivity", Phys. Rev. Lett. 84, 4184 (2000).
[62] S. A. Ramakrishna, "Physics of negative refractive index materials", Rep. Prog. Phys. 68, 449 (2005).
[63] Y. Zeng, X. Chen, W. Lu, "Optical limiting in defective quadratic nonlinear photonic crystals", J. Appl. Phys. 99, 123107 (2006).
[64] Y. Zeng, Y. Fu, X. Chen, W. Lu, and H. Ågren, "Highly efficient generation of entangled photon pair by spontaneous parametric down-conversion in defective photonic crystal", J. Opt. Soc. Am. B 24, 1365 (2007).
[65] W. L. Schaich, "Second harmonic genaration by periodically-structured metal surfaces", Phys. Rev. B 78, 195416 (2008).
[66] M. Corvi, W. L. Schaich, "Hydrodynamic-model calculation of second-harmonic generation at a metal surface", 33, 3688 (1986).
[67] W. L. Schaich, A. Liebsch, "Nonretarded hydrodynamic-model calculation of second-harmonic generation at a metal surface", Phys. Rev. B 37, 6187 (1988).
[68] A. Liebsch, W. L. Schaich, "Second-harmonic generation at simple metal surfaces", Phys. Rev. B 40, 5401 (1989).
[69] Y. Liu, G. Bartal, D. A. Genov, X. Zhang, "Subwavelength Discrete Solitons in Nonlinear Metamaterials", Phys. Rev. Lett. 99, 153901 (2007).
[70] S. Feng, K. Halterman, "Parametrically Shielding Electromagnetic Fields by Nonlinear Metamaterials", Phys. Rev. Lett. 100, 063901 (2008).
[71] A. A. Zharov, I. V. Shadrivov, Y. S. Kivshar, "Nonlinear Properties of Left-Handed Metamaterials", Phys. Rev. Lett. 91, 037401 (2003).
[72] M. Scalora, M. S. Syrchin, N. Akozbek, E. Y. Poliakov, G. DAguanno, N. Mattiucci, M. J. Bloemer, A. M. Zheltikov, "Generalized Nonlinear Schrödinger Equation for Dispersive Susceptibility and Permeability: Application to Negative Index Materials", Phys. Rev. Lett. 95, 013902 (2005).
[73] A. T. Georges, "Coherent and incoherent multiple-harmonic generation from metal surfaces", Phys. Rev. A 54, 2412 (1996).
[74] However, in the spirit of the quasi-monochromatic assumption the spectra around the second harmonic should be correct. The wrong low-frequency contribution must be confined to frequencies at most twice the spectral width of the exciting pulse.